Journal of Computational and Applied Mathematics 429 (2023) 115210

Contents lists available at ScienceDirect

Journal of Computational and Applied Mathematics

journal homepage: www.elsevier.com/locate/cam

NIMOC: A design and analysis tool for supersonic nozzles under non-ideal compressible flow conditions

Marta Zocca [a,*], Paolo Gajoni [b], Alberto Guardone [b]

[a] Laboratory of Fluid Dynamics, LUT University, Yliopistonkatu 34, Lappeenranta, 53850, Finland
[b] Department of Aerospace Science & Technology, Politecnico di Milano, Via La Masa 34, Milan, 20156, Italy

ARTICLE INFO

Article history:
Received 31 October 2022
Received in revised form 19 February 2023

Keywords:
Supersonic nozzle
Non-ideal compressible fluid dynamics
Method of characteristics

ABSTRACT

A computational tool for non-ideal supersonic nozzle flows is developed to perform direct design of nozzle geometries and flow analysis of shock-free off-design conditions. So-called non-ideal flows are characterized by the departure of the fluid thermodynamics from the ideal-gas law, which is the case of supersonic expansions close to the critical point, either in the superheated vapour or in the supercritical region. Deviations from the ideal-gas model of remarkable significance are observed in connection with, but not limited to, fluids made of complex molecules. NIMOC (Non-Ideal Method Of Characteristics) implements a formulation of the Method Of Characteristics (MOC) valid for non-ideal flows: the classical formulation of the MOC is complemented with state-of-the-art nonlinear multiparameter Equations of State (EoS) implemented in external thermodynamic libraries. NIMOC implements a two-dimensional and axisymmetric formulation of the MOC, which is applied to the solution of the isentropic expansion through nozzles of different geometrical configurations: straight-axis symmetric and axisymmetric conventional wind-tunnel nozzles, straight-axis symmetric and axisymmetric minimum-length nozzles, and asymmetric nozzles with curved meanline. Results are presented, which demonstrate nozzle design and flow analysis in the presence of paradigmatic non-ideal flow phenomena. Verification of MOC computations is performed by means of inviscid Computational Fluid Dynamics (CFD) simulations and experimental data. Results are presented for selected geometrical configurations.

1. Introduction

In many technical applications, mainly in the sectors of power conversion [1,2] and transportation of high-pressure fluids [3], the behaviour of fluid flows significantly departs [4] from the ideal-gas or the ideal-liquid models. Elaborate and computationally expensive models based on highly nonlinear multiparameter equations of state [5] are required in order to predict the thermophysical properties of such flows. In all mentioned applications, an accurate prediction of thermophysical properties is essential for adequate design and fluid dynamic analysis of components and systems, see e.g. Ref. [6].

A thermodynamic property which discriminates between ideal and non-ideal flow behaviour is the so-called fundamental derivative of gasdynamics, defined by Thompson (1971) [7] as:

$$\Gamma = 1 + \frac{c}{v}\left(\frac{\partial c}{\partial P}\right)_s, \tag{1}$$

* Corresponding author.
E-mail address: marta.zocca@lut.fi (M. Zocca).

https://doi.org/10.1016/j.cam.2023.115210

where v and P are the local specific volume and pressure of the fluid. The variable Γ represents a nondimensional measure of the variation of the speed of sound with pressure along an isentropic expansion. Based on the value of Γ, so-called ideal or ideal-like ($\Gamma > 1$) and non-ideal ($0 < \Gamma < 1$) flow regimes can be defined. In the ideal regime, the speed of sound increases with pressure, which is the behaviour of usual substances. In the non-ideal regime, the speed of sound decreases with pressure, which is the behaviour displayed by several molecularly complex fluids of industrial application when operating in the vicinity of the saturated vapour curve and critical point [8]. Among these fluids, there exists a class which displays negative values of Γ in the same thermodynamic region. The flow regime characterized by $\Gamma < 0$ is termed non-classical.

A complete classification of flow regimes is outside of the scope of the present work, and the interested reader can consult Refs. [4,7,9]. For the purpose of the present discussion, it is sufficient to highlight the influence of Γ on the flow through de Laval nozzles operating in the non-ideal regime, which is the main focus of the present study. The thermodynamic variable Γ governs the evolution of the flow field in de Laval nozzles, entailing remarkable consequences on the design and operation of such gasdynamic devices in the non-ideal regime. For a perfect gas, Γ is constant regardless of the thermodynamic state and evaluates to $\Gamma = (\gamma + 1)/2$, which is always greater than 1. The value of Γ depends only on the characteristics of the working fluid through the (constant) value of the specific heat ratio γ. If a more complex Equation of State (EoS) is adopted to compute the thermophysical properties of the flow, Γ is computed using either Eq. (1) or other derived formulations, resulting in expressions which feature an explicit dependence on the local thermodynamic state of the fluid. Thermodynamic libraries are available nowadays, such as CoolProp [10] and FluidProp [11,12], which implement the procedures to compute Γ using state-of-the-art EoS for a wide range of fluids and operating conditions. The local thermodynamic state along an isentropic nozzle expansion in the non-ideal regime depends on the reservoir conditions. Such dependence on the reservoir conditions is embedded in the evolution of Γ along the expansion process. As a consequence, while in the ideal-gas regime nozzles are designed for a particular working fluid and exhaust Mach number (or, equivalently, for an assigned reservoir-to-exhaust pressure ratio), in the non-ideal regime nozzles are designed for a particular working fluid, exhaust Mach number (or reservoir-to-exhaust pressure ratio), and for a specific reservoir thermodynamic state.

A mature numerical technique for the design and flow analysis of supersonic nozzles is the Method of Characteristics (MOC). The MOC, which is a solution method for hyperbolic equations, provides a technique for designing the contour of the diverging section of a de Laval nozzle so that a shock-free flow is attained, taking into account the multidimensional flow inside the duct. Despite the current advancements in Computational Fluid Dynamics (CFD) and computational design methodologies, the MOC is still widely adopted in diverse technical applications as a direct design method for supersonic nozzles, as demonstrated by recent published studies in the fields of rocket propulsion [13] and power conversion systems [14]. Moreover, the MOC is still the subject of active research in connection with non-ideal flows, see e.g. Ref. [15]. Despite its well-established role as a direct design method, the advantage of using the MOC as an analysis method for supersonic flows instead of a CFD analysis of the same level of fidelity is instead debatable and it needs to be assessed on a case-by-case basis, especially if non-ideal flows are considered. Due to the computational power and the advanced CFD tools available nowadays, the time required to setup and run a non-ideal MOC analysis from scratch could be comparable with the time required to pre-process and run an inviscid CFD simulation with non-ideal thermodynamics. While MOC-based computations using the ideal-gas or simple cubic EoS usually require less than 1 s on standard computers available at time of writing, computing times may increase up to several minutes if multiparameter EoS are used.

In line with the interest of the scientific community towards MOC-based techniques, this work presents a software, named NIMOC (Non-Ideal Method Of Characteristics), which implements a comprehensive and modular methodology capable of performing the design, geometrical sizing and flow analysis for several types of de Laval nozzles in the non-ideal flow regime. De Laval nozzles are the simplest benchmark fluid dynamic devices to model and experimentally characterize non-ideal expansions. Moreover, converging–diverging ducts with uniform inlet flow and supersonic outflow are the simplest geometries representative of blade passages of supersonic turbomachinery. Due to the wide range of applicability of the nozzle flow schematization, the software is intended both as a research tool for investigating non-ideal supersonic expansions and as an aid for engineers and practitioners to perform the design and analysis of supersonic expanders in the power conversion and propulsion sectors. Existing codes implementing the MOC for non-ideal flows mostly focus on one particular type of nozzle geometry, or on the planar and axisymmetric configuration of the same geometry [15–18]. In NIMOC, the methodologies for solving the two-dimensional and axisymmetric isentropic expansions through conventional straight-axis planar and axisymmetric nozzles, both with smooth and sharp-cornered throat, are combined. In addition to the implementation of a unified design and analysis procedure for straight-axis nozzles operating in non-ideal conditions, this work introduces two benchmark geometrical configurations for planar nozzles with a curved meanline, with supersonic turbomachinery intended as the main target technical application. The design and analysis procedures for such planar asymmetric nozzle shapes are developed and verified.

The paper is structured as follows. In Section 2, the MOC-based procedures for nozzle design and analysis are illustrated. In Section 3, both the analysis and design procedures are verified by comparing NIMOC's predictions with reference CFD results and experimental data. Grid independence studies for the MOC are presented first. Second, test cases are presented, which demonstrate the application of the MOC to nozzles of different geometries and in paradigmatic non-ideal conditions. Section 4 provides final remarks.

2. Method of characteristics (MOC) for non-ideal flows

Throughout the paper, the reference flow schematization is that of a planar/axisymmetric nozzle operating under chocked flow conditions and performing a steady isentropic expansion from the reservoir thermodynamic state to supersonic conditions. As a further assumption, the flow is considered as inviscid and adiabatic. Moreover, a shock-free flow field is assumed. Within this framework, the specific total enthalpy per unit mass h^{t} and specific entropy per unit mass s can be assumed uniform over the entire flow field, and the governing equations for steady compressible irrotational flows apply:

$$\begin{aligned} &(u^2 - c^2)u_x + (u^2 - c^2)v_y + 2uvu_y - \delta\frac{c^2 v}{y} = 0 \\ &u_y - v_x = 0 \end{aligned} \tag{2}$$

where (x, y) are the spatial coordinates, (u, v) are the flow velocity components, subscripts indicate partial derivatives, c is the speed of sound, and δ is a constant parameter that allows to switch from the axisymmetric model ($\delta = 1$) to the planar model ($\delta = 0$).

The fluid thermodynamics enters the governing equations only through the definition of the speed of sound, which can be derived from an appropriate Equation of State (EoS). In the present case of uniform total enthalpy h^{t} and entropy s, the speed of sound is a function of the velocity module $\|\mathbf{u}\|$ only, and the following relation holds:

$$c^2 = c^2(s, h) = c^2\left(s, h^t - \frac{\|\mathbf{u}\|^2}{2}\right) = c^2(\|\mathbf{u}\|^2) \tag{3}$$

The governing equations Eq. (2) are elliptic for $M < 1$, and they become hyperbolic for $M > 1$, thus enabling the application of the MOC for their solution. Specifically, the solution to the governing equations is sought only in the divergent section, where the flow is supersonic, pursuing two main goals. Design routines calculate the flow field in order to compute a geometry of the divergent section that delivers a parallel uniform flow at nozzle exhaust, while analysis routines are aimed at computing the flow field in an assigned divergent geometry.

The MOC is a well-known and consolidated technique, which allows to reduce the solution of the governing partial differential equations (PDE) Eq. (2) to the solution of a set of ordinary differential equations (ODE) holding only along the so-called characteristic lines. Specifically, the characteristic lines are defined by the ordinary differential equations:

$$\frac{\mathrm{d}y}{\mathrm{d}x} = \lambda_{\pm}, \tag{4}$$

where $\lambda_{\pm} = \tan(\vartheta \pm \alpha)$ is the slope of the characteristic lines, ϑ is the local direction of the flow, and $\alpha = \sin^{-1}(1/M)$ is the Mach angle. Along the characteristic lines $C^{\pm}$ defined by Eq. (4), the following compatibility equations apply:

$$(u^2 - c^2)\mathrm{d}u_{\pm} + [2uv - (u^2 - c^2)\lambda_{\pm}]\mathrm{d}v_{\pm} - \delta\frac{c^2 v}{y}\mathrm{d}x_{\pm} = 0, \tag{5}$$

where the differentials $\mathrm{d}u$, $\mathrm{d}v$, and $\mathrm{d}x$ are evaluated along the characteristic lines.

The formulation of the MOC introduced so far and continuing in the following sections closely follows the presentation and nomenclature proposed by Zucrow & Hoffman 1977 [19]. First, one identifies whether a certain computing station is internal to the flow field, along a solid boundary, or along a symmetry axis, so to apply the appropriate series of specific computations, called unit processes. As it will be illustrated in Section 2.3, the MOC computations are a downstream-marching sequence of unit processes, which must start from an independent solution capable of predicting the flow field up to a downstream location—typically slightly downstream of the geometrical throat—where the flow is everywhere supersonic. Initialization methods for the MOC implemented in NIMOC are presented in Section 2.2.

2.1. Computation of thermodynamic properties

As commented at the beginning of Section 2, the fluid thermodynamics enters the governing equations only through the definition of the speed of sound. Nevertheless, the implementation of the MOC for the general non-ideal case entails the complication of computing each thermodynamic property using highly nonlinear EoS. Moreover, characterizing the dependence of the flow variables on the flow velocity $\|\mathbf{u}\|$ requires the numerical solution of the energy conservation law $h + \|\mathbf{u}\|^2/2 = h^{\mathrm{t}}$, since the well-known closed-form isentropic relations valid in the ideal-gas regime are not valid for non-ideal flows, see e.g. [20].

Both the ideal-gas and the van der Waals EoS are coded in NIMOC. More general and accurate non-ideal EoS are included through the interface towards the external thermodynamic libraries CoolProp [10] and FluidProp [11]. Moreover, NIMOC includes a lookup table (LuT) approach for the computation of thermophysical properties. The derived thermodynamic properties are calculated from the input pairs (P, T), (P, s), and (h, s) using the CoolProp or RefProp [21] libraries. Moving from the promising results obtained by previous investigators in the simulation of single-phase non-ideal flows [22], LuT based on unstructured grids are adopted, instead of more conventional tabulations based on cartesian

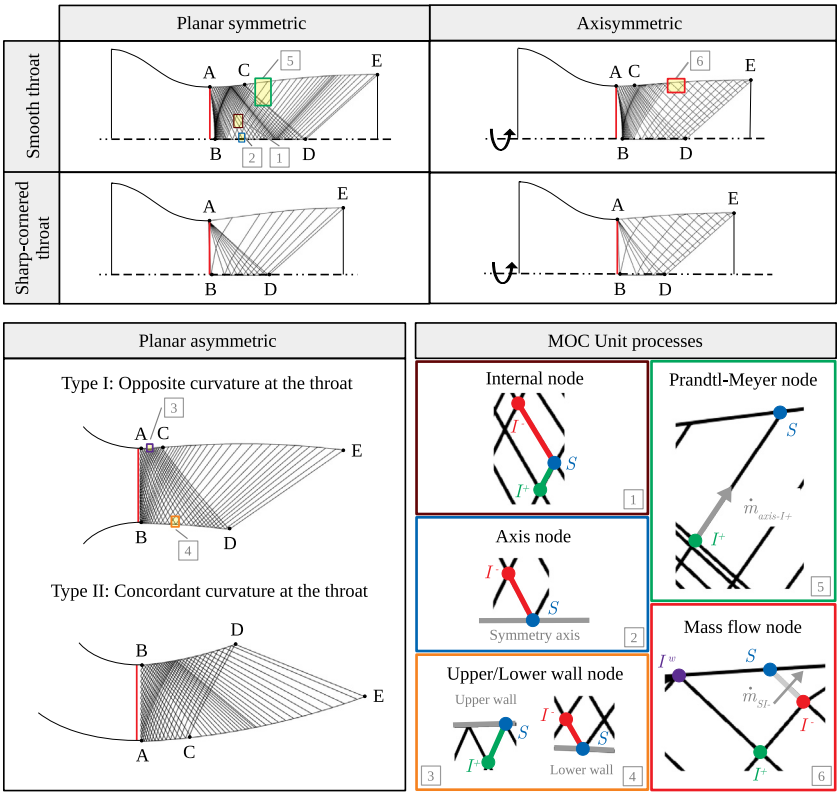

Fig. 1. Schematization of the design procedure for all types of nozzles. MOC unit processes are schematized in the bottom-right box. Unit processes are labelled from 1 to 6 to mark the regions of the flow where they are applied.

grids. The input pairs represent the two-dimensional coordinates of the nodes of a triangular unstructured mesh, which is generated for a given range of input properties using a fully-automated procedure. The derived thermodynamic properties at any query point over the input range are computed using linear interpolation. Specifically, a barycentric coordinate interpolation scheme is applied along the triangular grid element containing the query point, in order to reconstruct the derived thermodynamic property based on the values of the same property at the vertices of the triangle. The use of unstructured LuT could represent a valid alternative to the direct call to EoS especially in the case of transcritical expansion. Transcritical expansions cross the thermodynamic region close to the critical point and around the critical isotherm, which is a region characterized by large gradients in the thermodynamic properties. In addition to the high computational cost of the resolution of complex EoS, such large gradients in thermodynamic properties entail significant practical challenges in the numerical modelling of transcritical expansions, since they often cause the solvers of EoS to diverge. At those baseline grid points where the direct computation of the derived thermodynamic properties fails due to the divergence of the thermodynamic solver, the values of the derived properties are reconstructed from the derived properties at neighbouring grid points using an inverse distance weighting algorithm. An accuracy assessment and grid independence study of the LuT approach implemented in NIMOC is presented in Section 3.1.2.

2.2. Initialization of the MOC

An independent solution of the transonic flow in the throat region of the nozzle is required to start the MOC computations in the supersonic divergent section. Such transonic solution can either be read by NIMOC as an external input or it can be computed using analytical hard-coded procedures, which are illustrated in the following. In the former case, the solution of the flow field in the convergent and in the throat region of the nozzle can be obtained, for example, from CFD calculations or from solution methods valid for subsonic and transonic flows. The initial-data line for the MOC can be passed to NIMOC as a set of spatial coordinates (x, y), where the flow velocity vector $\mathbf{u} = (u, v)$ is known. Hard-coded analytical procedures, instead, are used to compute the transonic flow in the throat region of the nozzle based on formulations presented by previous investigators. Such formulations are specific to the geometrical configuration of the nozzle. In Fig. 1, all the nozzle geometries considered in NIMOC are displayed. For all nozzles, the position of the geometrical throat, which also sets the origin of the x axis, is highlighted with a red vertical line, while the black curves represent the characteristics net. The origin of the y axis is located instead along the symmetry axis for planar nozzles,

and along the meanline at the geometrical throat for asymmetric nozzles. The initial-data curve is identified as curve AB for all geometries. For planar symmetric and axisymmetric nozzles, the transonic solution $\mathbf{u}(x, y)$ is computed using the formulation of Sauer [23], which is a linearized solution of the governing equations Eq. (2) obtained by applying a small-perturbation technique. The throat section is made of a circular arc of (dimensional) radius R_t. The transonic velocity field reads:

$$\mathbf{u}(\hat{x}, y) = \begin{pmatrix} u(\hat{x}, y) \\ v(\hat{x}, y) \end{pmatrix} = \|\mathbf{u}\| \begin{pmatrix} 1 + \alpha\hat{x} + \dfrac{\bar{\Gamma}\alpha^2\hat{x}y}{1+\delta} \\ \dfrac{2\bar{\Gamma}\alpha^2\hat{x}y}{1+\delta} + \dfrac{2\bar{\Gamma}^2\alpha^3}{(3+\delta)(1+\delta)}y^3 \end{pmatrix} \tag{6}$$

where δ is the discriminant between the planar and axisymmetric solution (see Section 2 and Eq. (2)) and the parameters $\hat{x}$ and α read:

$$\begin{aligned} \hat{x} &= x - \frac{1}{3}\bar{\Gamma}\alpha H^2, \\ \alpha &= \sqrt{\frac{1}{2\bar{\Gamma}R_\mathrm{t}}}, \end{aligned} \tag{7}$$

In Eqs. (6) and (7), $\bar{\Gamma}$ is the value of the fundamental derivative of gasdynamics computed at the sonic state, while H is the throat semi-height. According to the linearized solution of Sauer, the sonic line is an arc of a parabola (see e.g. Fig. 6 in the results section), which crosses the geometrical throat and displays its most aft location along the symmetry axis of the nozzle. The equation of the initial-data line (curve AB on Fig. 1) is the locus of points characterized by a null velocity component in the vertical direction $v = 0$. Along the $v = 0$ line the flow is entirely supersonic.

For planar and axisymmetric sharp-cornered nozzles, the determination of the centred expansion occurring at the throat location is initiated by assuming a straight sonic line at the geometrical throat. This assumption, adopted both in classical textbooks [20] and in a recent implementation of the non-ideal MOC [15], provides a reasonable estimate of the layout of the transonic flow only if the convergent displays a gentle curvature close to the nozzle throat section.

For planar asymmetric nozzles, two benchmark geometrical configurations, defined as Type I and Type II geometry in Fig. 1, are identified. For both the Type I and the Type II geometries, the upper and lower contours of the throat section are defined by circular arcs of dimensional radii $R_{\mathrm{t,up}}$ and $R_{\mathrm{t,low}}$, respectively. While for Type I geometries the lower throat contour has negative curvature, for Type II geometries the lower throat contour has positive curvature. For both Type I and Type II configurations, the transonic solution of Syvertson and Savin [24] can be applied to the determination of the initial-data line. The solution of Syvertson and Savin extends the method proposed by Sauer for the transonic solution of the flow field around an airfoil, which in turn adopts the same hypotheses and solution method as seen for planar and axisymmetric nozzles. The MOC is initialized, for both Type I and Type II geometries, along a straight vertical line drawn from the most aft axial location of the sonic line, which is again an arc of a parabola (see e.g. Fig. 6 in the results section). Along the straight vertical line marked as curve AB in Fig. 1, the flow is entirely supersonic. The velocity field in the throat section is given by:

$$\begin{aligned} \mathbf{u}(x, \hat{y}) &= \begin{pmatrix} u(x, \hat{y}) \\ v(x, \hat{y}) \end{pmatrix} \\ &= \|\mathbf{u}\| \begin{pmatrix} 1 + \alpha x + -\beta\hat{y} + \hat{y}^2\left(\bar{\Gamma}\alpha^2 + \beta^2\right) \\ -\beta x + x\hat{y}\left(2\beta^2 + 2\bar{\Gamma}\alpha^2\right) \\ -\hat{y}^2\left[\alpha\beta\bar{\Gamma} + 4\beta x\left(\bar{\Gamma}\alpha^2 + \beta^2\right)\right] + \hat{y}^3\frac{1}{3}\bar{\Gamma}^2\alpha^3 \end{pmatrix}, \end{aligned} \tag{8}$$

where the parameters α and β read:

$$\begin{aligned} \alpha &= \frac{1}{2\bar{\Gamma}}\left[\frac{1}{H}\left(\frac{1}{R_{\mathrm{t,up}}} - \frac{1}{R_{\mathrm{t,low}}}\right) - \frac{1}{R_{\mathrm{t,up}}^2}\right], \\ \beta &= \frac{1}{R_{\mathrm{t,up}}}, \end{aligned} \tag{9}$$

$\bar{\Gamma}$ is the value of the fundamental derivative of gasdynamics computed at the sonic state, and $\hat{y} = y - H$. In Eq. (9), $R_{\mathrm{t,up}}$ is always positive for both Type I and Type II geometries, while $R_{\mathrm{t,low}}$ is negative for Type I geometries, positive for Type II ones. In the remainder of the paper, the initialization methods presented so far are identified by the acronym ATS, which stands for Approximate Transonic Solutions.

For planar symmetric and asymmetric nozzles, an alternative way to obtain the initial-data line is provided by the Streamline Curvature Method (SLC). It is a well-established iterative method born in the turbomachinery field and belonging to the family of throughflow methods, which are widely used in the preliminary design and in the quasi-3D analysis of compressor and turbine flows. The interested reader can consult Refs. [25–28] for further details. In this kind of methods, a three-dimensional compressible flow, modelled as steady, adiabatic and inviscid, is restricted on stream surfaces, in order to simplify the governing equations. A simplified version of the method is here applied to two-dimensional nozzles to simulate the flow within the convergent and the throat region. The SLC method, in fact, features

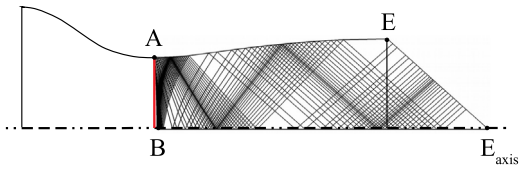

Fig. 2. Schematization of the analysis procedure.

convergence problems for supersonic flows, whereas it provides fast and reliable results for subsonic and transonic flows. State of-the-art non-ideal EoS can be included through the interface towards the external thermodynamic library FluidProp [11]. The flow velocity vector $\mathbf{u} = (u, v)$ along a line slightly after the geometric throat, where the flow is entirely supersonic, is extracted from the solution and it is passed to NIMOC as initial-data line. Further details about the method implementation are reported in Appendix.

2.3. Nozzle design

For nozzles of all types, input to the design routines are the reservoir conditions, the working fluid, the selected thermodynamic model (cf. Section 2.1), the geometry of the throat ($R_{\text{t,up}}$, $R_{\text{t,low}}$) and the design parameter. The latter can be the exhaust Mach number, the reservoir-to-exhaust pressure ratio, the exhaust static pressure, or the specific enthalpy drop across the nozzle.

To illustrate the design procedures implemented in NIMOC, the nozzles featuring a smooth throat profile are examined first. Once the initial-data line (curves AB in Fig. 1) is determined, the upper (lower—for asymmetric nozzles of Type II) portion of the divergent geometry immediately downstream of the geometrical throat is assigned as a circular arc of radius $R_{\text{t,up}}$ ($R_{\text{t,low}}$ for Type-II asymmetric nozzles). The flow field in region ACDB is completely determined by the reservoir conditions, by the initial data, and by the assigned wall geometry. The expansion flow field is governed by Eq. (2), which are solved numerically using the MOC. In this region, the internal flow is solved using the Internal node unit process (see Fig. 1): once the flow field at two points in the flow (I^+, I^-) is known, the solution at a third point S can be found. Wall points, and symmetry axis points for symmetric nozzles, are instead determined using the Upper/Lower wall node and the Axis node unit processes (see again Fig. 1): if the conditions at a point in the flow near a solid wall (I^+ for the Upper wall node, I^- for the Lower wall node) or at a symmetry axis (I^-) are known, then the flow variables at a point on the wall/at the symmetry axis (S) can be found. The design outflow parameter is attained at the locations marked with letter D on Fig. 1. Curve AC defines the so-called expansion region of the nozzle, i.e. the region in which expansion to the desired outflow parameter is performed. The portion CE of the divergent is termed turning region, since it is devoted to the generation of a parallel uniform flow at nozzle exhaust. In the exhaust flow field, characteristics are straight lines, whose slope is determined by the exhaust Mach number. The exit section is immediately obtained by requiring the mass flow rate across line DE to be equal to the mass flow rate across the initial value line AB, where E is a straight characteristic drawn from point D. The turning profile CE is determined by imposing the mass flow rate through each discrete characteristic line intersecting the nozzle wall. The flow in the area enclosed within points CDE is a simple-wave region for all planar nozzles, while it is a two-family region for axisymmetric nozzles. For all planar nozzles, the turning region is determined by finding the termination point of each C^+ characteristic (C^- for planar asymmetric nozzles of Type II) emanating from curve CD, based on the mass balance requirement. The corresponding unit process is called Prandtl–Meyer node in Fig. 1. For axisymmetric nozzles instead, the flow field along line DE constitutes, together with the flow along curve CD, the initial dataset for the computation of the flow in the region CDE. The marching of the characteristic net from line DE towards the upper wall of the nozzle is arrested once the mass balance requirement is satisfied. The unit process for the determination of the turning region for axisymmetric nozzles is identified as Mass flow node in Fig. 1.

For sharp-cornered nozzles, the marching of the characteristic net in the centred expansion downstream of line AB is arrested at point D along the symmetry axis, where the design conditions are met. The turning region is constructed following the same procedure illustrated for planar and axisymmetric nozzles.

2.4. Flow analysis

Flow analysis using the MOC on a given geometry is now described. For nozzles of all types, input to the design routines are the reservoir conditions, the working fluid, the selected thermodynamic model (cf. Section 2.1), and the coordinates of the divergent profile(s). In the case of sharp-cornered nozzles, also the off-design outflow condition is required to set the limiting downstream characteristic of the centred expansion at the throat. A schematization of the flow analysis procedure is illustrated in Fig. 2 only with reference to planar symmetric nozzles. The procedure is the same for all geometries. From the reservoir conditions and the nozzle geometry, the initial-data line AB is determined. The solution of the flow field in the region $\text{AEE}_{\text{axis}}\text{B}$ proceeds as illustrated in Section 2.3 for the expansion region ACDB. The downstream marching of the characteristic net is stopped when the end point E of the nozzle contour is reached.

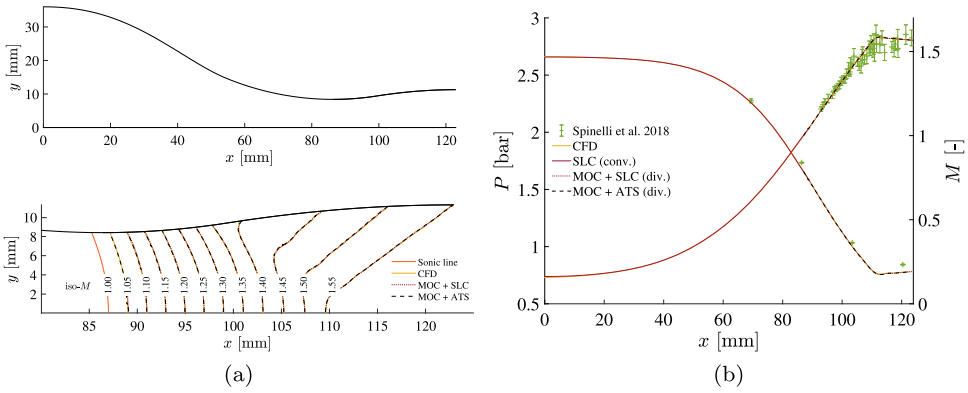

Fig. 3. Verification of the MOC and SLC analysis procedures against reference inviscid CFD simulations (CFD, iPRSV) and experimental data (Spinelli et al. 2018): geometry of the nozzle (Fig. 3(a), top), Mach number isolines from $M = 1.05$ to $M = 1.5$ in the divergent section (Fig. 3(a), bottom), pressure and Mach number profiles along the nozzle axis (Fig. 3(b)).

3. Results and discussion

3.1. Verification of the method and grid independence studies

In this section, the implementation of the MOC is verified by performing the flow analysis of a supersonic expansion of siloxane fluid MDM (Octamethyltrisiloxane, $C_8H_{24}O_2Si_3$) in a nozzle of known geometry, and comparing MOC computations with reference experimental and CFD results. In the selected process conditions, which fall within the non-ideal flow regime, the nozzle operates off design.

3.1.1. Method of characteristics

The planar symmetric nozzle displayed in the top half of Fig. 3(a) constitutes the test section of the TROVA blow-down wind tunnel of CREALab, Politecnico di Milano, Italy [29]. The supersonic flow of MDM in the diverging portion of the nozzle is computed with the MOC. Input data for NIMOC are the total pressure 2.69 bar, the total temperature 263 °C, the coordinates of the divergent section, and the radius of the throat section. The latter datum is used to compute the transonic solution in the throat region required to initialize the MOC (cf. Eq. (6) and (7) in Section 2.2). The geometry of the nozzle, as well as experimental data of pressure and Mach number distribution along the axis of the nozzle for the studied operating conditions are available from Ref. [29]. Reference CFD simulations on this same geometry and similar operating conditions were performed by Gori et al. [30], which set the methodology and tools used in the present study for running the CFD simulation presented as comparison with the MOC results.

The bottom half of Fig. 3(a) shows the diverging portion of the nozzle, where a comparison of the Mach isolines obtained from the MOC and from an inviscid CFD simulation is carried out. The MOC computation is initialized with 100 data points on the initial-data line, while the CFD simulation is run using the open-source software SU2 [31] and an unstructured triangular mesh of 60k nodes. The computational domain of the CFD simulation includes both the convergent and the divergent sections of the nozzle. Characteristics-based boundary conditions are adopted: input properties are total pressure, total temperature, and an outlet static pressure which is set to establish a supersonic outflow from the nozzle. Both the MOC and the CFD analyses are complemented with the iPRSV EoS [32]. In Fig. 3(b), the pressure and Mach number profiles along the axis of the nozzle, from inlet to outlet, are shown. The MOC results are compared with CFD, alongside the reference experimental data documented in Ref. [29]. From Fig. 3(a) and from Fig. 3(b), it is observed that the MOC results overlap the CFD analysis both along the symmetry axis, where the direction of the flow is well defined and one-dimensional, and in the rest of the flow field, where the flow is fully two-dimensional. Since both methods solve the Euler equations within the nozzle, albeit without the hypothesis of irrotationality in the case of CFD, the overlapping of results is not relevant per se, but it is an expected outcome that indicates a correct implementation of the MOC. The solution of the flow in the converging portion of the nozzle obtained with the SLC method is also included in Fig. 3(b) for verification.

The normalized root mean square error (NRMSE) evaluated with respect to reference solutions of SLC and MOC in the converging and diverging portions of the nozzle, respectively, are reported in Fig. 4. Pressure, Mach number, velocity, and density are extracted along the axis of the nozzle. The SLC and MOC are run with an increasing number of data points along the initial-data line, while the reference solutions are obtained with 300 data points. For all the monitored properties, the NRMSE between the candidate and the reference solutions show a converging trend at increasing number of data points. In the remainder of the paper, results obtained with 100 data points are provided, since this number of data points represents a fair trade-off between the accuracy of the analysis and the computing time.

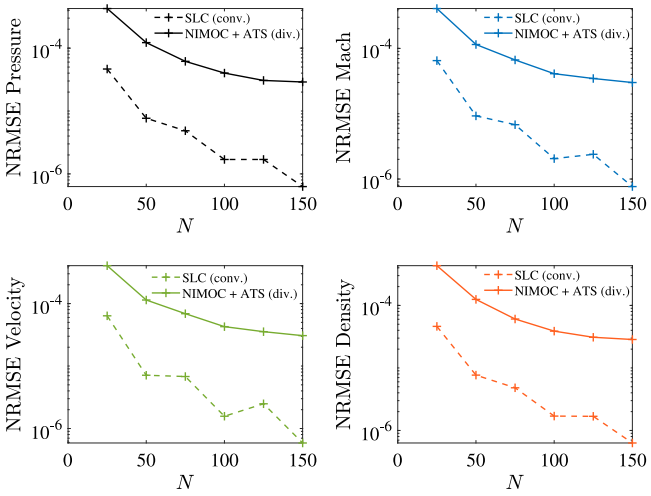

Fig. 4. MOC and SLC grid convergence in terms of the normalized root mean square error (NRMSE) of pressure, Mach number, velocity, and density along the nozzle axis, evaluated with respect to reference solutions.

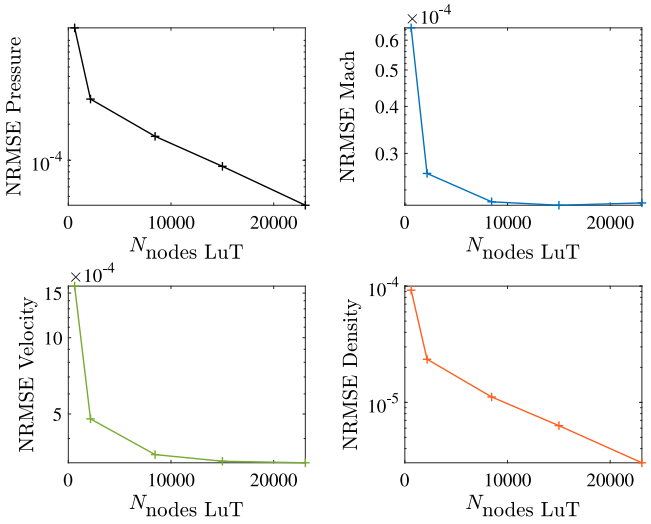

Fig. 5. Grid convergence of the LuT approach in terms of the normalized root mean square error (NRMSE) of pressure, Mach number, velocity, and density along the nozzle axis, evaluated with respect to a reference MOC calculation run with direct solution of the Span–Wagner EoS.

3.1.2. LuT approach

A grid independence study for the LuT approach is now presented. The same flow analysis presented in Section 3.1.1 is carried out using both direct computation of the thermodynamic properties and LuT of different grid resolution. The number of data points along the initial-data line is 100, and the EoS used in both approaches is the Span–Wagner EoS with parameters defined by Thol et al. [33], i.e. the EoS for MDM implemented in the CoolProp library. The NRMSE between selected flow variables computed using the LuT approach and the direct computation are reported in Fig. 5. Pressure, Mach number, velocity, and density are extracted along the axis of the nozzle from the reference simulation run with direct computation of the thermodynamic properties and from LuT simulations carried out at increasing resolution of the LuT. All the monitored properties follow a converging trend at increasing number of nodes of the unstructured LuT, and a satisfactory accuracy is reached for LuT of at least 10k nodes. In order to optimize the number of grid points, all LuT adopted in this test case are centred on the operating range of the nozzle. For this specific case, a resolution of 10k nodes corresponds to a spacing between temperature and pressure grid points of 0.1 K and 0.008 bar, respectively. LuT of higher number of nodes but similar spacing might be required if LuT including a wider operating range are adopted, possibly with the goal of simulating several different expansion processes using the same LuT. With the current implementation of the LuT procedure, no relevant performance advantage of the LuT approach with respect to the direct evaluation of the EoS was observed if LuT of adequate resolution were employed.

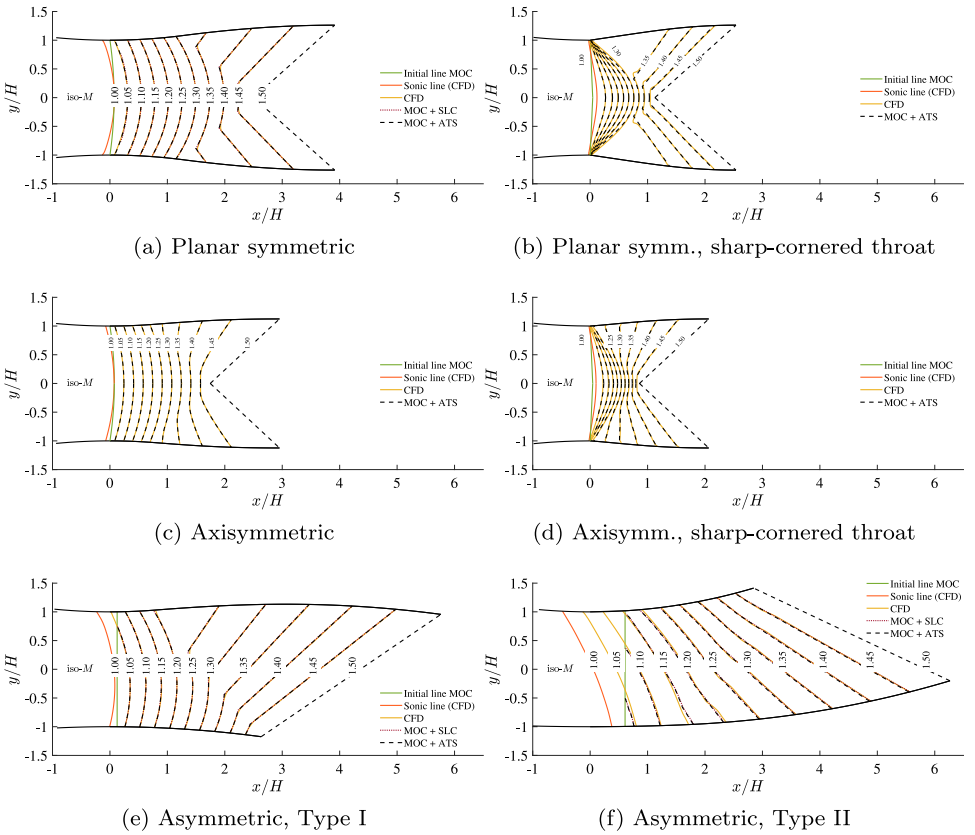

(a) Planar symmetric (b) Planar symm., sharp-cornered throat

(c) Axisymmetric (d) Axisymm., sharp-cornered throat

(e) Asymmetric, Type I (f) Asymmetric, Type II

Fig. 6. Verification of the MOC design procedure against reference inviscid CFD simulations (CFD, iPRSV). In all figures, the sonic line computed from CFD, the initial-data line of the MOC, and the Mach number isolines from $M = 1.05$ to $M = 1.5$ are reported.

3.2. Nozzle design and verification for different geometries

In this section, the verification of the procedures for nozzle design illustrated in Section 2.3 is carried out. Similarly to Section 3.1, MDM is considered as working fluid, and nozzles discharging from total conditions $(P^{\mathrm{t}}, T^{\mathrm{t}})$ of 2.69 bar and 263 °C are designed for all the different geometrical configurations implemented in NIMOC. All nozzles are designed to discharge a uniform parallel flow at an exhaust Mach number of 1.5. Thermodynamic properties are computed using the iPRSV EoS implemented in the FluidProp-StanMix library. The divergent sections designed with the MOC are shown in Fig. 6. For nozzles with smooth throat (symmetric, axisymmetric, and asymmetric – Fig. 6(a), Fig. 6(c), Fig. 6(e), and Fig. 6(f), respectively), the upper curvature of the throat section is assigned to $R_{\mathrm{t,up}} = 10H$, while for asymmetric nozzles the lower curvature of the throat section is assigned to $R_{\mathrm{t,low}} = -20H$ for Type I (Fig. 6(e)) and to $R_{\mathrm{t,low}} = 40H$ for Type II (Fig. 6(f)).

On Fig. 6, the isolines of the flow Mach number computed with the MOC are compared to the Mach isolines resulting from inviscid CFD simulations. CFD simulations are run on unstructured triangular grids using the SU2 solver and the iPRSV EoS, similarly to the reference CFD simulations presented in Section 3.1. The computational domains of CFD simulations include both the divergents designed with the MOC and the convergents. Specifically, the convergents (not shown) deliver a horizontal flow at the inlet section of each nozzle, and match the throat section with a circular arc of the same radius as the throat radius. For sharp-cornered planar and axisymmetric nozzles, the same convergents generated for their counterparts with smooth throat are adopted. Mach isolines resulting from MOC and CFD overlap fairly well in all geometries, indicating that the design procedure implemented in NIMOC yields an adequate shape of the divergent section, which is capable of delivering a parallel uniform flow for the design outflow condition.

Fig. 6 also reports the sonic ($M = 1$) lines, obtained from CFD simulations, and the MOC initial-data lines. By comparing the relative positions of the sonic lines with the corresponding initial-data lines, it is possible to assess the suitability of the MOC initialization methods implemented in NIMOC (see Section 2.2). For planar symmetric and axisymmetric nozzles (Fig. 6(a) and Fig. 6(c)), the transonic solution of Sauer (1947) provides qualitatively and quantitatively accurate initial data, at least in the simulated cases, which satisfy Sauer's hypothesis of $R_{\mathrm{t}} \gg H$. From Fig. 6(a) and Fig. 6(c), it is observed that the maximum displacement of the sonic line from the geometrical throat computed from CFD intersects the initial

data line of the MOC at the symmetry axis. This result indicates that the sonic line predicted by Sauer's solution, which is used to define the initial-data line as described in Section 2.2, overlaps the CFD solution. For planar asymmetric nozzles (Fig. 6(e), and Fig. 6(f)), the transonic solution of Syvertson & Savin (1953) provides less accurate yet acceptable initial data for the MOC. Similarly to Sauer's solution, Syvertson & Savin's formulation is valid when the throat radii are significantly larger than the throat height. This requirement is fulfilled in the present case study. For the asymmetric nozzle of Type I (Fig. 6(e)), the maximum displacement of the sonic line resulting from CFD does not overlap the position of the initial-data line of the MOC. However, the $M = 1.05$ isoline computed from the MOC, which directly emanates from the initial-data line, overlaps the one resulting from CFD. A similar conclusion can be drawn by observing the results of Fig. 6(f), i.e. the results for planar asymmetric nozzles of Type II. In this latter case, the mismatch between the most aft streamwise location along the sonic line (CFD) and the position of the initial-data line (MOC) is more relevant. However, the solution along the initial-data line is seen to predict the flow in the low-supersonic regime fairly well, since the $M = 1.05$, 1.10, and 1.15 isolines emanating from the initial-data line are matched with satisfactory accuracy. Finally, sharp-cornered nozzles (Fig. 6(b) and Fig. 6(d)) are considered. Due to the gentle curvature of the convergent in the proximity of the throat section, the assumption of a straight sonic line is deemed reasonable in this case study, despite a noticeable qualitative difference between the MOC initial-data line and the CFD solution. However, as commented for the planar asymmetric nozzles, the MOC and the CFD solutions are seen to overlap from the low-supersonic regime ($M = 1.05$) to the exhaust section.

3.3. Nozzle design in paradigmatic non-ideal conditions

The design of nozzles operating in paradigmatic non-ideal conditions is presented in this section. For the first example, the working fluid is siloxane MM (Hexamethyldisiloxane, $C_6H_{18}OSi_2$), which is expanded from total pressure and temperature of 29 bar, 265 °C to an exhaust Mach number of 1.7, which corresponds to an exhaust pressure of ∼5 bar. In the selected process conditions, a nonmonotone variation of the flow Mach number along the expansion is expected. Indeed, EoS accounting for the non-ideal behaviour of the flow, such as the van der Waals EoS and the Span–Wagner EoS with parameters defined by Thol et al. [34], predict that the flow Mach number may decrease at decreasing density for a set of thermodynamic states along the studied isentropic expansion. Such prediction is based on the quasi-one-dimensional theory for non-ideal nozzle flows (see e.g. [35]). For quasi-one-dimensional flows with uniform entropy and total enthalpy, the flow Mach number M can be expressed as function of the density ρ only, with s and h^{t} acting as constant parameters:

$$M(\rho; s, h^{\mathrm{t}}) = \frac{u(\rho; s, h^{\mathrm{t}})}{c(s, \rho)} = \frac{\sqrt{2\,[h^{\mathrm{t}} - h(s, \rho)]}}{c(s, \rho)} \tag{10}$$

Derivation of the above relation with respect to density yields:

$$\frac{\mathrm{d}M}{\mathrm{d}\rho}(\rho; s, h^{\mathrm{t}}) = \frac{M(\rho; s, h^{\mathrm{t}})}{\rho} J(\rho; s, h^{\mathrm{t}}) \tag{11}$$

where the function $J(\rho; s, h^{\mathrm{t}})$ is defined as:

$$J(\rho; s, h^{\mathrm{t}}) = 1 - \Gamma(s, \rho) - \frac{1}{M^2(\rho; s, h^{\mathrm{t}})} \tag{12}$$

For thermodynamic states satisfying $\Gamma > 1$, M is a monotone decreasing function of density ($J < 0$). For $0 < \Gamma < 1$, the Mach number is a decreasing function of density if $J < 0$, and an increasing function of density if $J > 0$. The limiting condition $J = 0$ marks the stationary points of the $M(\rho)$ function:

$$M(\rho; s, h^{\mathrm{t}})_{J=0} = \sqrt{\frac{1}{1 - \Gamma(\rho; s, h^{\mathrm{t}})}} \tag{13}$$

For the operating conditions examined here, the Mach number given by Eq. (13) is always greater than 1, which means that the Mach number can attain a non-monotone profile only in the divergent section of the nozzle.

The design routines of NIMOC, complemented with the ideal-gas, the van der Waals, and the Span–Wagner EoS yield the divergent shapes shown in Fig. 7. Spatial coordinates (x, y) are made nondimensional with the throat height H. The colour scale provides the distribution of the flow Mach number in the divergent section. The profiles of fundamental derivative of gasdynamics Γ, density ρ, streamwise velocity u, speed of sound c, flow Mach number M, and pressure P along the axes of the three divergent sections of Fig. 7 are reported. The results obtained with the van der Waals and with the Span–Wagner EoS are considered first. In accordance with the quasi-one-dimensional theory of non-ideal flow expansions, while density (Fig. 8(b)) and pressure (Fig. 8(f)) monotonically decrease, and the flow velocity (Fig. 8(c)) monotonically increases, the speed of sound displays a nonmonotone trend (Fig. 8(d)), which in turn determines the nonmonotone profiles of the flow Mach number reported in Fig. 8(e). For thermodynamic states characterized by $\Gamma > 1$, the speed of sound decreases along the expansion (cf. Fig. 8(a) and Fig. 8(d)), while for states having $\Gamma < 1$ the speed of sound is observed to increase. In the ideal-gas case, in which Γ is constant and > 1, all flow variables vary monotonically, in accordance with conventional gasdynamics theory.

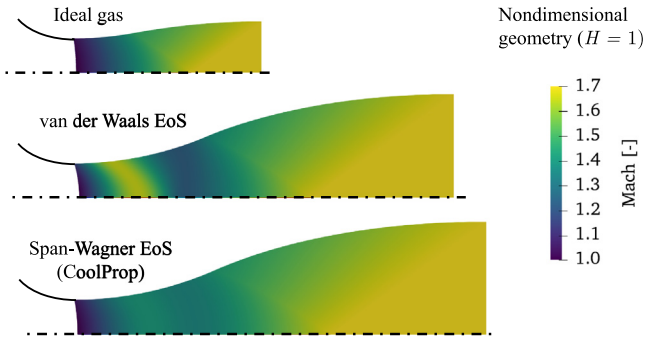

Fig. 7. Divergent shapes resulting from MOC design in conditions yielding a nonmonotone Mach number profile in the divergent. Results are shown in nondimensional geometry, scaled with the throat semi-height.

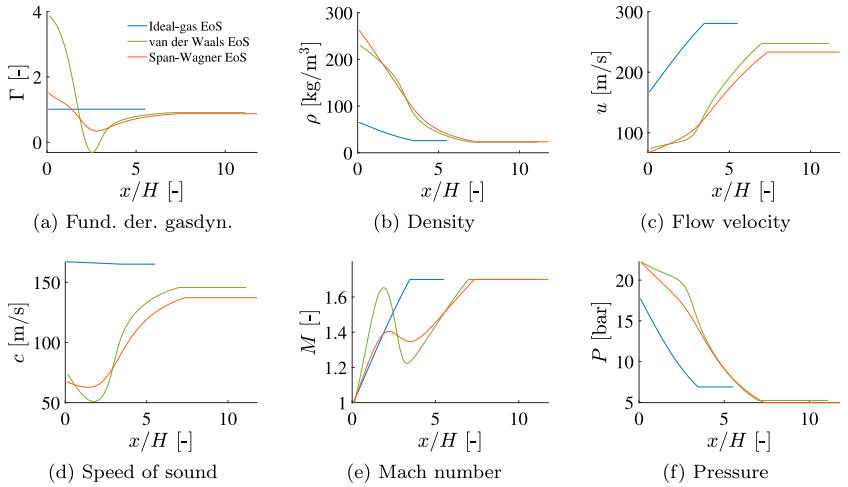

Fig. 8. Profiles of selected flow variables along the nozzle axis. Results are obtained from MOC design performed in conditions yielding a nonmonotone Mach number distribution in the divergent.

The divergent shapes reported in Fig. 9 result from dimensional scaling of the divergent shapes of Fig. 7. Scaling is performed by imposing a discharged mass flow rate $\dot{m} = 1$ kg/s and a channel depth $d = 2$ mm to all studied nozzles. By comparing the nondimensional divergent shapes of Fig. 7 with the scaled shapes of Fig. 9, it is immediate to observe that the difference in overall size between the nozzles designed with the ideal-gas EoS and the ones designed with non-ideal EoS is less remarkable in the scaled geometries. Indeed, the scaling performed using the ideal-gas EoS yields a throat height which is almost twice as larger as the throat height obtained using non-ideal EoS. Several concurrent factors determine the size and shape of supersonic nozzles in the presence of significant non-ideal flow effects. The quasi-one-dimensional theory provides a relation between the gradients of the flow variables and the area gradient of the nozzle geometry. Specifically, the equation relating the streamwise Mach number gradient with the area gradient reads:

$$\frac{1}{M}\frac{dM}{dx} = \frac{1+(\Gamma-1)M^2}{M^2-1}\frac{1}{A}\frac{dA}{dx} \tag{14}$$

Except for the portion of divergent immediately after the throat, where $\Gamma > 1$ also in the non-ideal case (cf. Fig. 8(a)), the term multiplying the area gradient is always greater for the ideal-gas case ($\Gamma = 1.0128$) than for the non-ideal case. This implies that the streamwise Mach number gradient $\mathrm{d}M/\mathrm{d}x$ in the non-ideal gas case is lower than the one obtained in the ideal-gas case, thus resulting in a lower area gradient $\mathrm{d}A/\mathrm{d}x$. Moreover, the non-ideal pressure profiles of Fig. 8(f) show a less steep pressure decrease than the ideal-gas case, although monotonicity is preserved. In summary, the slower evolution of the flow variables towards the desired outflow conditions observed in the non-ideal case influences the shape—but not the scaling—of the nozzle through an overall decrease of the area gradient, or, equivalently, an increase of the nozzle length.

For both ideal and non-ideal flows, the geometrical scaling depends ultimately on the reservoir conditions, since the sonic flow parameters used for dimensional sizing explicitly depend on the reservoir property pair. However, while in the non-ideal case the qualitative evolution of the expansion changes at changing the position of the reservoir conditions (and

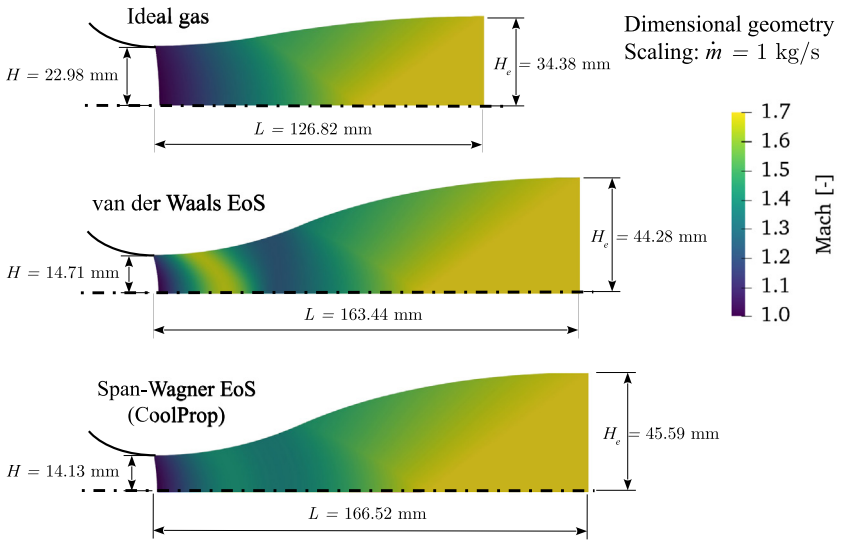

Fig. 9. Divergent shapes resulting from MOC design in conditions yielding a nonmonotone Mach number profile in the divergent. Results are shown in dimensional geometry, namely scaled for $\dot{m} = 1$ kg/s and channel depth 2 mm.

therefore of the process isentrope) in the thermodynamic plane, the qualitative features of an ideal-gas expansion do not change regardless of the reservoir state. Indeed, a well-known feature of ideal-gas flows is that the static flow properties are in constant ratios with respect to the corresponding reservoir conditions, these ratios being dependent only on the properties of the working fluid through the constant specific heat ratio γ.

While demonstrating the capability of NIMOC to capture unconventional non-ideal phenomena, the test case presented in this section stresses the importance of including geometrical scaling routines into non-ideal nozzle design procedures, in order to fully assess the relevance of non-ideal phenomena on the final design of the nozzle.

Finally, nozzle designs for three fluids of increasing molecular complexity are presented to observe benchmark non-ideal flow patterns typical of each class of fluid. The three fluids considered here, namely carbon dioxide (CO_2), hexamethyldisiloxane (MM, $C_6H_{18}OSi_2$), and dodecamethylcyclohexasiloxane (D6, $C_{12}H_{36}O_6Si_6$) are representative of Low Molecular Complexity (LMC) fluids, High Molecular Complexity (HMC) fluids, and Bethe-Zel'dovich-Thompson (BZT) fluids (see the classification proposed by Colonna and Guardone [9]). CO_2 is expanded from total pressure and temperature of 300 bar, 500 °C ($P^t/P_c = 4.0675$, $T^t/T_c = 2.5422$), MM, is expanded from 29.5 bar, 265 °C ($P^t/P_c = 1.4956$, $T^t/T_c = 1.0374$), and D6 is expanded from 10.74 bar, 378.7 °C ($P^t/P_c = 1.1171$, $T^t/T_c = 1.0094$). For all three fluids, nozzle design is initialized from the flow field computed in the converging section using the SLC method. All nozzles are designed for an exhaust Mach number of 1.75.

Fig. 10 displays the resulting nozzle shapes in nondimensional units and the profiles of the flow Mach number M and of the parameter J (see Eq. (12)) extracted along the centreline. The designs and profiles obtained using the ideal-gas model are compared to the ones computed using multiparameter EoS. For CO_2 (Fig. 10(a)), $\Gamma > 1$ along the entire expansion. Deviations between ideal and non-ideal behaviour are only quantitative and due to the non-ideal thermodynamic behaviour of the fluid in the supercritical region. The profile of the flow Mach number is monotone throughout the nozzle. Results reported for MM in Fig. 10(b) are obtained for an expansion occurring in the non-ideal thermodynamic region ($0 < \Gamma < 1$). The process conditions and the resulting non-monotone Mach number profile observed in the diverging portion of the nozzle were extensively examined in the first part of this section. Here, Fig. 10(b) highlights the correlation between the observed nonmonotone behaviour of M and the parameter J, which for LMC fluids can turn positive only for $M > 1$, namely in the divergent section of the nozzle. Finally, the behaviour displayed in Fig. 10(c) can only be observed in BZT fluids. Along the expansion of D6 considered in this example, thermodynamic states characterized by a negative value of Γ are reached, and the parameter J is seen to turn positive in the subsonic portion of the flow, leading to a non-monotone distribution of the flow Mach number along the converging portion of the nozzle.

4. Conclusions

A design and analysis tool for supersonic nozzles based on the Method of Characteristics (MOC) was implemented and tested in diverse operating conditions under the non-ideal compressible flow regime. State-of-the-art multiparameter Equations of State were adopted to describe the fluid thermodynamics in both the design and analysis procedures. MOC-based computations were successfully verified against reference inviscid numerical simulations for all geometries, namely

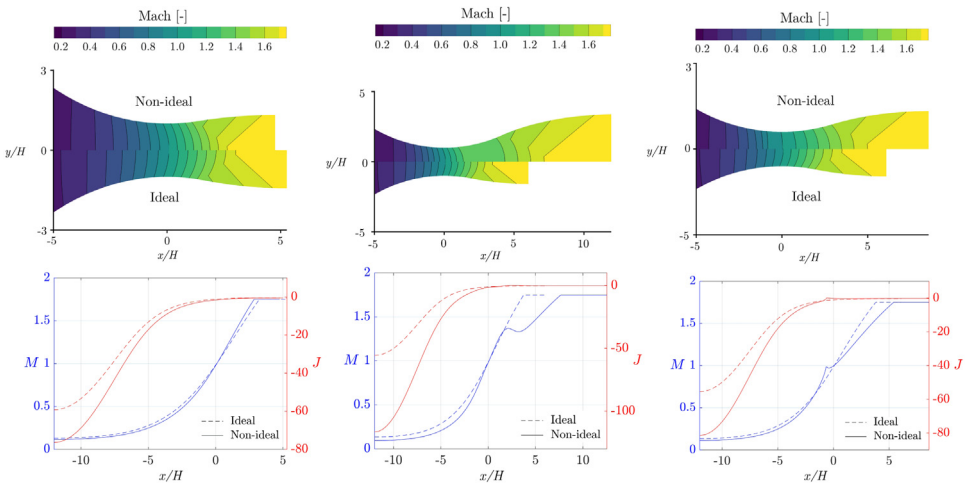

Fig. 10. Nozzle designs for fluids CO_2 (a), MM (b), D6 (c), representative of LMC, HMC, and BZT classes, respectively. Mach number isolines and profiles of flow Mach number and parameter J (Eq. (12)) are reported. Non-ideal thermodynamic properties are computed using the Span-Wagner EoS.

straight-axis symmetric and axisymmetric conventional wind-tunnel nozzles, straight-axis symmetric and axisymmetric minimum-length nozzles, and asymmetric nozzles with curved meanline. The coded design procedure proved capable of reproducing paradigmatic non-ideal flow phenomena, which have a significant influence on the shape and geometrical scaling of the nozzle walls. Specifically, the importance of including geometrical scaling routines into non-ideal nozzle design procedures was stressed. The examined test cases demonstrated that the non-ideal fluid thermodynamics influences the designed nozzle geometry both in terms of nondimensional parameters such as the exhaust-to-throat area ratio and the normalized length of the nozzle, and in terms of the dimensional scaling of the whole divergent geometry, which ultimately depends on the process conditions. The coded analysis procedure, which possibly includes both the convergent and the divergent sections of the nozzle if the MOC is used in connection with the SLC method, provides a prediction of the flow field of comparable level of fidelity and accuracy as inviscid CFD.

Data availability

The authors are unable or have chosen not to specify which data has been used.

Acknowledgements

This research was partially funded by Academy of Finland, Finland under grant number 342135, project *Non-ideal compressible flows in turbomachinery*.

Appendix. Streamline Curvature Method for the initialization of the MOC

The Streamline Curvature Method is an iterative computational method based on the solution of the compressible Euler equations for steady flows. Negligible heat transfer and viscous effects are assumed, therefore both the specific total enthalpy h^t and entropy s per unit mass are conserved along streamlines. Cumulative effects of the viscosity can be explicitly added into the solution by means of viscous models, to account for dissipative phenomena such as friction and shock losses.

The main equation, derived from the compressible Euler equations, is the normal momentum equation (NME), namely a momentum equation projected along a direction roughly normal to streamlines. The computational grid is based on fixed stations, also called quasi-orthogonals, along which the momentum equation is solved, and floating streamlines. The streamlines are guessed at the beginning of the calculation and they are allowed to float based on the NME solution, in order to satisfy continuity in each streamtube, except for the streamlines following the nozzle walls, which are kept fixed. An example of computational mesh for the convergent and the throat region of the nozzle is shown in Fig. A.11, where the quasi-orthogonals are set as vertical lines and the number of streamlines is strongly reduced to increase the figure readability.

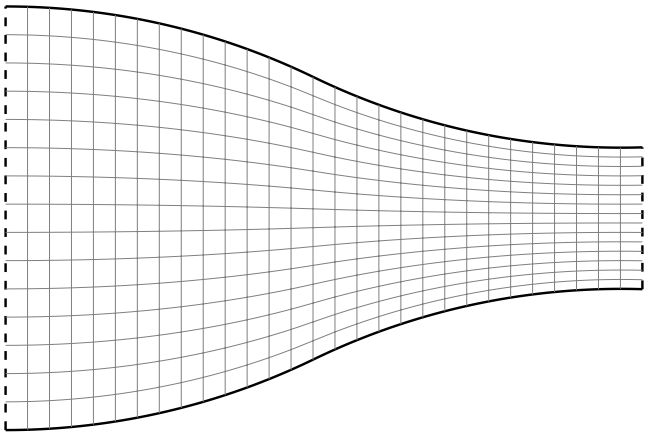

Fig. A.11. Computational grid for the SLC method.

The normal momentum equation is derived from its more general formulation [36], which is valid for quasi-3D flows. Neglecting the terms related to the dissipative effects, the NME reads

$$\frac{\partial u_\ell}{\partial q} = -\frac{\cos\phi}{r_c} u_\ell + \sin\phi \, \frac{\partial u_\ell}{\partial \ell}. \tag{A.1}$$

In the above expression, the coordinates q and ℓ follow the quasi-orthogonal and the streamline, respectively, u_ℓ is the flow velocity in the streamline direction, r_c is the local radius of curvature of the streamline and ϕ is the angle between the streamline and the direction normal to the quasi-orthogonal. Since the quasi-orthogonals are set to vertical lines, for simplicity, the coordinate q can be replaced by y, considering a cartesian flow representation. Eq. (A.1) can be written as an ordinary differential equation (ODE) as

$$\frac{du_\ell}{dy} + A(y)u_\ell = B(y), \tag{A.2}$$

where the parameters $A(y)$ and $B(y)$ are computed at each iteration from the streamlines location and the solution at the previous step.

An analytical solution of Eq. (A.2) can be found as sum of a homogeneous and a particular solution, yielding

$$u_\ell(y) = e^{-\int_{y_0}^{y} A(y')dy'} \cdot \left[u_\ell(y_0) + \int_{y_0}^{y} B(y') e^{\int_{y_0}^{y'} A(y'')dy''} dy' \right], \tag{A.3}$$

where y_0 is set at the lower wall of the nozzle. The solution starts with the guessed value of $u_\ell(y_0)$ and is then integrated along the entire section of the nozzle. The NME is solved in conjunction with the continuity equation,

$$\dot{m} = \int_{y_0}^{y_{up}} \rho u_\ell \cos\phi dy, \tag{A.4}$$

being y_{up} the coordinate of the upper wall, which is solved for each station to satisfy mass conservation. Due to the constancy of total enthalpy h^{t} and entropy s, the density ρ in the above expression is a function of the velocity module $\|\mathbf{u}\| = u_\ell$ only,

$$\rho = \rho(s, h) = \rho\left(s, h^t - \frac{\|\mathbf{u}\|^2}{2}\right) = \rho(\|\mathbf{u}\|^2) = \rho(u_\ell^2), \tag{A.5}$$

and it is computed from the ideal-gas EoS or from more sophisticated non-ideal EoS through the thermodynamic library FluidProp.

Since the flow has to expand in supersonic conditions throughout the divergent, choking conditions are imposed at the throat. Hence, the mass flow rate $\dot{m}$ is set to its critical value $\dot{m}_c$, computed from the quasi-1D approximation of nozzle flows, namely

$$\dot{m} = \dot{m}_c = \rho^* u^* A_t, \tag{A.6}$$

where A_t is the throat area and the star superscript specifies that the quantities are evaluated in sonic conditions ($M = 1$). The quasi-1D solution is also used as initial guess to start the computation.

Due to the iterative nature of the method and the high non-linearity of the normal momentum equation, care is needed in the solution procedure. In order to successfully obtain the final solution, the streamline displacement at each iteration is therefore damped to improve solver robustness.

References

[1] P. Colonna, E. Casati, C. Trapp, T. Mathijssen, J. Larjola, T. Turunen-Saaresti, A. Uusitalo, Organic Rankine cycle power systems: From the concept to current technology, applications and an outlook to the future, ASME J. Eng. Gas Turbines Power 137 (2015) 100801.
[2] K. Brun, P. Friedman, R. Dennis, Fundamentals and Applications of Supercritical Carbon Dioxide (SCO_2) Based Power Cycles, first ed., Elsevier, 2017.
[3] E. Jassim, M.A. Abdi, Y. Muzychka, Computational fluid dynamics study for flow of natural gas through high-pressure supersonic nozzles: Part 1. Real gas effects and shockwave, Petrol. Sci. Technol. 26 (15) (2008) 1757–1772.
[4] A. Kluwick, Non-ideal compressible fluid dynamics: A challenge for theory, J. Phys. Conf. Ser. 821 (1) (2017) 012001.
[5] R. Span, W. Wagner, Equations of state for technical applications. I. Simultaneously optimized functional forms for nonpolar and polar fluids, Int. J. Thermophys. 24 (1) (2003) 1–39.
[6] M. White, A.I. Sayma, C.N. Markides, Supersonic flow of non-ideal fluids in nozzles: An application of similitude theory and lessons for ORC turbine design and flexible use considering system performance, J. Phys. Conf. Ser. 821 (2017) 012002.
[7] P.A. Thompson, A fundamental derivative in gasdynamics, Phys. Fluids 14 (9) (1971) 1843–1849.
[8] B. Brown, B. Argrow, Application of Bethe–Zel'dovich–Thompson fluids in organic Rankine cycle engines, J. Propuls. Power 16 (6) (2000) 1118–1124.
[9] P. Colonna, A. Guardone, Molecular interpretation of nonclassical gasdynamics of dense vapors under the van der Waals model, Phys. Fluids 18 (5) (2006) 56101–56114.
[10] I.H. Bell, J. Wronski, S. Quoilin, V. Lemort, Pure and pseudo-pure fluid thermophysical property evaluation and the open-source thermophysical property library CoolProp, Ind. Eng. Chem. Res. 53 (6) (2014) 2498–2508.
[11] P. Colonna, T.P. van der Stelt, FluidProp: A Program for the Estimation of Thermophysical Properties of Fluids, Energy Technology Section, Delft University of Technology, The Netherlands, 2005, http://www.fluidprop.com.
[12] P. Colonna, N.R. Nannan, A. Guardone, T.P. van der Stelt, On the computation of the fundamental derivative of gas dynamics using equations of state, Fluid Phase Equilib. 286 (1) (2009) 43–54.
[13] A.K. Flock, A. Gülhan, Design of converging-diverging nozzles with constant-radius centerbody, CEAS Space J. 12 (2020) 191–201.
[14] N. Anand, P. Colonna, M. Pini, Design guidelines for supersonic stators operating with fluids made of complex molecules, Energy 203 (2020) 117698.
[15] J.C. Restrepo, A.F. Bolaños-Acosta, J.R. Simões-Moreira, Short nozzles design for real gas supersonic flow using the method of characteristics, Appl. Therm. Eng. 207 (2022) 118063.
[16] A. Guardone, A. Spinelli, V. Dossena, Influence of molecular complexity on nozzle design for an organic vapor wind tunnel, ASME J. Eng. Gas Turbines Power 135 (2013) 042307.
[17] E. Bufi, P. Cinnella, Preliminary design method for dense-gas supersonic axial turbine stages, J. Eng. Gas Turbines Power 140 (2018).
[18] N. Anand, S. Vitale, M. Pini, G.J. Otero, R. Pecnik, Design methodology for supersonic radial vanes operating in nonideal flow conditions, J. Eng. Gas Turbines Power 141 (2) (2018) 022601.
[19] M.J. Zucrow, J.D. Hoffman, Gas Dynamics. Volume 2 – Multidimensional Flow, John Wiley and Sons, Inc., New York, 1977.
[20] J.D. Anderson, Modern Compressible Flow: With Historical Perspective, third ed., McGraw Hill Higher Education, 2004.
[21] E.W. Lemmon, I.H. Bell, M.L. Huber, M.O. McLinden, NIST Standard Reference Database 23: Reference Fluid Thermodynamic and Transport Properties-REFPROP, Version 10.0, National Institute of Standards and Technology, 2018.
[22] A. Rubino, M. Pini, M. Kosec, S. Vitale, P. Colonna, A look-up table method based on unstructured grids and its application to non-ideal compressible fluid dynamic simulations, J. Comput. Sci. 28 (2018) 70–77.
[23] R. Sauer, General Characteristics of the Flow Through Nozzles at near Critical Speeds, TM 1147, NACA, 1947.
[24] C.A. Syvertson, R.C. Savin, The Design of Variable Mach Number Asymmetric Supersonic Nozzles by Two Procedures Employing Inclined and Curved Sonic Lines, TM 2922, NACA, 1953.
[25] D. Frost, A streamline curvature through-flow computer program for analysing the flow through axial-flow turbomachines, 1970.
[26] D. Wilkinson, Calculation of blade-to-blade flow in a turbomachine by streamline curvature, 1970.
[27] M. Casey, C. Robinson, A new streamline curvature throughflow method for radial turbomachinery, J. Turbomach. (2010).
[28] J. Hu, H. Ou-Yang, X. ZHu, X. Qiang, Z. Du, An improved streamline curvature approach for transonic axial compressor performance prediction, Proc. Inst. Mech. Eng. G 225 (5) (2011) 575–584.
[29] A. Spinelli, G. Cammi, S. Gallarini, M. Zocca, F. Cozzi, P. Gaetani, V. Dossena, A. Guardone, Experimental evidence of non-ideal compressible effects in expanding flow of a high molecular complexity vapor, Exp. Fluids 59 (126) (2018) 70–77.
[30] G. Gori, M. Zocca, G. Cammi, A. Spinelli, P.M. Congedo, A. Guardone, Accuracy assessment of the non-ideal computational fluid dynamics model for siloxane MDM from the open-source SU2 suite, Eur. J. Mech. B/Fluids 79 (2020) 109–120.
[31] F. Palacios, M.F. Colonno, A.C. Aranake, A. Campos, S.R. Copeland, T.D. Economon, A.K. Lonkar, T.W. Lukaczyk, T.W.R. Taylor, J.J. Alonso, Stanford University unstructured (SU2): An open-source integrated computational environment for multi-physics simulation and design, in: 51st AIAA Aerospace Sciences Meeting and Exhibit, 2013.
[32] T.P. van der Stelt, N.R. Nannan, P. Colonna, The iPRSV equation of state, Fluid Phase Equilib. 330 (2012) 24–35.
[33] M. Thol, F.H. Dubberke, E. Baumhögger, J. Vrabec, R. Span, Speed of sound measurements and fundamental equations of state for octamethyltrisiloxane and decamethyltetrasiloxane, J. Chem. Eng. Data 62 (2017) 2633–2648.
[34] M. Thol, F.H. Dubberke, G. Rutkai, T. Windmann, A. Köster, R. Span, J. Vrabec, Fundamental equation of state correlation for hexamethyldisiloxane based on experimental and molecular simulation data, Fluid Phase Equilib. 418 (2016) 133–151.
[35] P.A. Thompson, Compressible-Fluid Dynamics, McGraw-Hill, 1988.
[36] P. Tiwari, A. Stein, Y. Lin, Dual-solution and choked flow treatment in a streamline curvature throughflow solver, J. Turbomach. 135 (4) (2013) 041004.